





## Article

# Study on the Surface Modification of Nanostructured Ti Alloys and Coarse-Grained Ti Alloys

Hsuan-Kai Lin <sup>1</sup>, Yi-Hong Cheng <sup>1</sup>, Guan-Yuan Li <sup>1</sup>, Ying-Chi Chen <sup>1</sup>, Piotr Bazarnik <sup>2</sup>, Jessica Muzy <sup>3</sup>, Yi Huang <sup>4,5,\*</sup> and Terence G. Langdon <sup>5</sup>

- <sup>1</sup> Graduate Institute of Materials Engineering, National Pingtung University of Science and Technology, Neipu 91201, Pingtung, Taiwan; hklin@mail.npust.edu.tw (H.-K.L.); xswzaq86248@gmail.com (Y.-H.C.); csb20491@gmail.com (G.-Y.L.); peic840228@gmail.com (Y.-C.C.)
- <sup>2</sup> Faculty of Materials Science and Engineering, Warsaw University of Technology, Woloska 141, 02-507 Warsaw, Poland; piotr.bazarnik@pw.edu.pl
- <sup>3</sup> School of Engineering in Physics, Electronics and Materials, Grenoble PHELMA, CEDEX 1, 38016 Grenoble, France; jessica.muzy1@grenoble-inp.org
- <sup>4</sup> Department of Design and Engineering, Faculty of Science and Technology, Bournemouth University, Poole BH12 5BB, UK
- <sup>5</sup> Materials Research Group, Department of Mechanical Engineering, University of Southampton, Southampton SO17 1BJ, UK; langdon@soton.ac.uk
- \* Correspondence: yhuang2@bournemouth.ac.uk; Tel.: +44-1202-961295

**Abstract:** Commercial purity titanium (CP-Ti) and a Ti-6Al-4V alloy (Ti64) were processed by high-pressure torsion (HPT) for 10 and 20 turns. The HPT processing produced a nanostructured microstructure and a significant strength enhancement in the CP-Ti and Ti64 samples. After 20 turns, the samples of HPT-processed CP-Ti and Ti64 were subjected to laser surface treatments in an air atmosphere using different scanning speeds and laser powers. The surface roughness of the laser-modified samples increased with increasing laser power and this produced hydrophilicity due to a lower contact angle. After a holding time of 27 days, these samples underwent a hydrophilic-to-hydrophobic transformation as the contact angle increased from 13° to as much as 120° for the CP-Ti sample, and for the Ti64 sample the contact angle increased from 10° to 126°. In addition, the laser surface modification process was carried out with different atmospheres (air, vacuum and O<sub>2</sub>) on heat-treated but unstrained CP-Ti and Ti64 samples and the contact angle changed due to the surface element content. Thus, as the carbon content increased from 28% to 47% in CP-Ti in a vacuum environment, the surface contact angle increased from 22° to 140°. When a laser surface modification process is conducted under oxygen-less conditions, it is concluded that the contact angle increases rapidly in order to control the hydrophobic properties of Ti and the Ti alloy.

**Keywords:** CP-Ti; high-pressure torsion; hydrophobic; laser surface modification; Ti-6Al-4V



**Citation:** Lin, H.-K.; Cheng, Y.-H.; Li, G.-Y.; Chen, Y.-C.; Bazarnik, P.; Muzy, J.; Huang, Y.; Langdon, T.G. Study on the Surface Modification of Nanostructured Ti Alloys and Coarse-Grained Ti Alloys. *Metals* **2022**, *12*, 948. <https://doi.org/10.3390/met12060948>

Academic Editor: Irina P. Semenova

Received: 19 February 2022

Accepted: 27 May 2022

Published: 31 May 2022

**Publisher's Note:** MDPI stays neutral with regard to jurisdictional claims in published maps and institutional affiliations.



**Copyright:** © 2022 by the authors. Licensee MDPI, Basel, Switzerland. This article is an open access article distributed under the terms and conditions of the Creative Commons Attribution (CC BY) license (<https://creativecommons.org/licenses/by/4.0/>).

## 1. Introduction

With the rapid development of modern science and technology, the introduction of new and modified materials has become attractive within materials science. Titanium alloys are a popular material for biomedical applications due to their high mechanical strength, excellent biocompatibility and good corrosion resistance [1–3]. There are reports where other elements are added to Ti alloys that this may enhance their properties by producing lower densities and improved biocompatibility and corrosion resistance [4]. In general, the mechanical properties of high-purity Ti are lower than for titanium alloys, such as the Ti-6Al-4V alloy, and, therefore, the mechanical strength is generally improved through the application of thermo-mechanical processing.

In practice, the application of severe plastic deformation (SPD) is a beneficial procedure for refining the grain structure and enhancing the mechanical strength of many metals

and alloys. For example, the procedures of accumulative roll-bonding (ARB) [5], equal-channel angular pressing (ECAP) [6] and high-pressure torsion (HPT) [7] are effective SPD procedures that have been used very extensively for achieving ultrafine-grain structures in a wide range of materials [8–13]. However, ECAP processing is normally conducted at a high temperature [14], whereas HPT processing can be carried out at room temperature due to the very high hydrostatic pressure, which prevents segmentation and cracking during the processing operation [15]. As a result, HPT is preferred in Ti alloys for achieving grain refinement and strength enhancement.

Wettability has an important role in a variety of surface-related phenomena and the surface characteristics of ultrafine-grained materials have a significant impact on their performance in industry and biomedicine [16,17]. Superhydrophobic surfaces have many attractive features, including self-cleaning, heat transfer and corrosion [18], and they are used widely in different fields, such as in anti-ice applications in aeronautics [19]. There are some reports of a difference between lotus leaves, which have recognized superhydrophobic surfaces, and the superhydrophobic effect associated with metallic surfaces because the effect in lotus leaves is due to their dual-scale roughness, at both the coarse micrometer and nanometer scales [20–22]. In addition, hydrophilic phenomena provide good tissue adhesion in implants and are designed for rapid cell–cell communications [22,23]. For example, a titanium alloy may be treated by acid etching or sandblasting to become bioactive and thereby, improve the connectivity between the bone implants and the surrounding tissue [24–26]. Obviously, therefore, surface modifications of engineering metals and alloys are essential in order to control and optimize their fundamental properties.

Various surface modification techniques are now available, including thermal spraying, mechanical treatment, chemical treatments, laser texturing and sol–gel processing. In practice, it has been demonstrated that laser modification is a useful tool for modifying the surface topography at the micro/nano scale [27–29] and, to date, there are reports demonstrating the feasibility of generating hydrophobic or hydrophilic characteristics on coarse-grained metals by laser surface machining [30,31]. Nevertheless, only a few studies are, at present, available, investigating the potential for combining both a modification of the surface properties and an improvement in the mechanical strength of ultrafine-grained Ti alloys [32]. The wetting behavior of a surface is significantly affected by the chemical composition and roughness, as described in the classic and early models of Wenzel [33] and Cassie-Baxter [34] and the wetting properties of Ti alloy are controlled by roughness so that the contact angle can be changed through two different states on rough solids [35]. It has been reported that after laser surface treatment the melted and re-solidified metal oxide on the surface can absorb organic compounds in ambient air leading to surface hydrophobicity [36–38]. Thus, as the observation period increases, so the contact angle also increases, and this means that the surface behavior changes from a hydrophilic to a hydrophobic state due to the local composition.

In general, it is apparent that high-energy metal oxides are generated during laser processing and this leads to hydrophilic behavior, so that the wettability of the surfaces changes over time from hydrophilicity to superhydrophobicity [39]. Most investigations to date have only explored tuning the wettability by laser texturing in an air atmosphere [40]. For example, it was shown that the processing atmosphere can accelerate or slow down the wettability transition, thereby extending the durability of the superhydrophilic surfaces [41], and it was also reported that wettability differences existed between samples processed under various atmospheres, so that the overall wettability tendencies were the result of a combination of surface chemistry and the topographic effects for all surfaces [42–45].

Due to limited information available to date on the laser surface modifications on nanostructured Ti alloys, the present study was initiated to examine the surface morphology of HPT-processed samples of pure Ti and a Ti-6Al-4V alloy after laser surface treatment, using different laser powers, speeds and holding times. This study will investigate different methods to fabricate a hydrophobic surface, which can be used in medical devices. An examination was also conducted to evaluate the effects of the chemical

compositions processed in different environments in creating either superhydrophilic or superhydrophobic surfaces.

## 2. Materials and Methods

A sample of grade 2 commercial purity (CP) titanium (99.4% Ti) was purchased from Titanium Industries UK, Ltd. (Birmingham, UK) in the form of a round bar with a diameter of 12.7 mm. A sample of the Ti-6Al-4V (Ti64) alloy was obtained from GoodFellow Cambridge Ltd. (Cambridge, UK), in the form of a round bar with a diameter of 10.0 mm. Typical composition analysis of Ti64 (in ppm) shows that it contains Fe 300, C 220, H 100, N 100 and O 650 in addition to Al 6% and V 4%. The as-received CP-Ti was annealed at 973 K for 2 h in a vacuum furnace and the as-received Ti64 was heat treated in two steps with an initial solution anneal at 1323 K for 45 min followed by stress relief annealing at 873 K for 3 h and then furnace cooling to room temperature. After the heat treatments, both the CP-Ti and the Ti64 rods were machined and cut into disc samples with diameters of 10 mm and thicknesses of ~0.8 mm [46].

Both the CP-Ti and the Ti64 disc samples were processed to totals of 10 or 20 turns by HPT at room temperature under an imposed pressure of 6.0 GPa using a rotational speed of 1 rpm. The principle of processing by HPT is illustrated schematically in Figure 1a [47]. The sample is generally in the form of a thin disc and it is placed between two massive anvils, subjected to a pressure  $P$  and then torsionally strained through rotation of either the lower or upper anvil. The HPT facility operated under quasi-constrained conditions where there is a small outflow of material around the periphery of the disc during the torsional straining [48,49]. Figure 1b shows the disc samples before and after HPT processing, with the flash at the edge of the disc after HPT processing. For CP-Ti and the Ti64 alloy, the heat-treated but unstrained samples are designated as N0 whereas the HPT-processed 10 and 20 turns samples are designated as N10 and N20, respectively. For optical microstructure observations of CP-Ti and Ti64, the samples were finally polished using a colloidal silica solution, then etched with Kroll reagent (2% HF + 10% HNO<sub>3</sub> + 88% H<sub>2</sub>O) for a few seconds. The optical microstructures of both CP-Ti and Ti64 samples were examined using an Olympus BX51 optical microscope (OM) (Olympus Corporation, Tokyo, Japan). The deformation microstructures of CP-Ti and Ti64 after 10 or 20 turns of HPT processing were characterized using a JEOL1200 transmission electron microscope (TEM) (JEOL Ltd., Tokyo, Japan) operating under an accelerating voltage of 120 kV. The standard 3 mm TEM disc samples were always taken from about 4 mm from the centres of the HPT-processed discs. The grain sizes of HPT-processed samples were measured using the linear intercept method with image J software (U.S. National Institutes of Health, Bethesda, MD, USA) with at least 30 grains measured from TEM images and the mean grain size value was used for comparison purposes. The microhardness was measured using a hardness tester equipped with a Vickers indenter (FM300, Future-tech Corporation, Kanagawa, Japan) under a load of 200 gf and with a dwell time of 15 s.

The surfaces of the HPT-processed samples were modified by laser surface texturing in an air atmosphere using various scanning speeds, laser powers and holding times in order to evaluate the influence of the various laser processing parameters on the surface roughness and hydrophilic/hydrophobic properties. The laser irradiations were performed on the heat-treated but unstrained samples in air, vacuum and O<sub>2</sub> atmospheres. The samples for laser treatment were hand rubbed against the abrasive papers first. Four grades of abrasive papers were used: 800 grit, 1200 grit, 2000 grit and 4000 grit. Then the samples were polished using alumina powder with a particle size of 0.3 µm. Prior to the laser surface texturing, the samples were further polished by alumina to a roughness of  $56 \pm 6$  nm. The samples were then surface treated using a fiber laser (SPI G3, SPI Lasers, Southampton, UK) with a wavelength of 1064 nm, a repetition rate of 25 kHz, a laser spot size of 40 µm and a pulse duration of >10 ns. The laser texturing process was carried out in power ranges of 0.9–5.0 W and with a scanning speed of 150 mm s<sup>-1</sup>. Figure 2 shows the configuration of the laser surface treatment system.

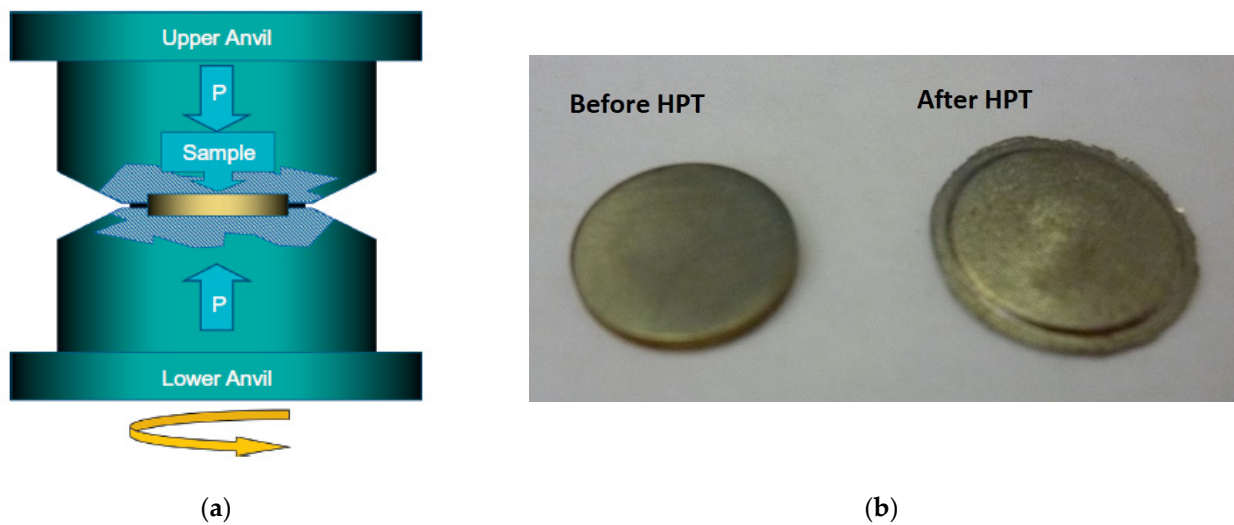


**Figure 1.** (a) Principle of HPT processing [47], (b) disc samples before and after HPT processing. Reprinted with permission from ref. [47]. Copyright 2022 Elsevier.

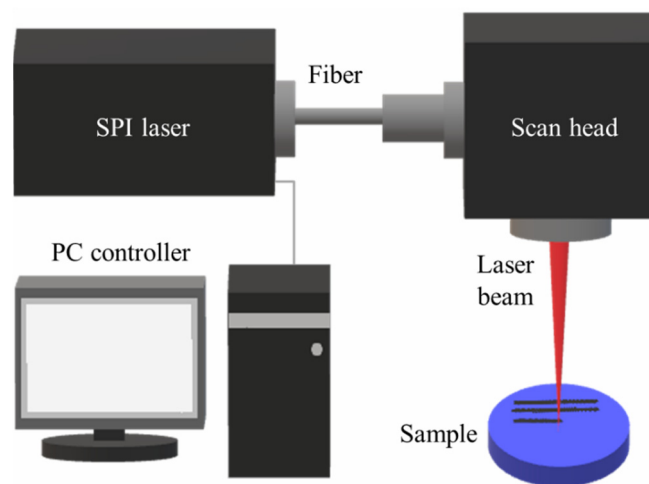
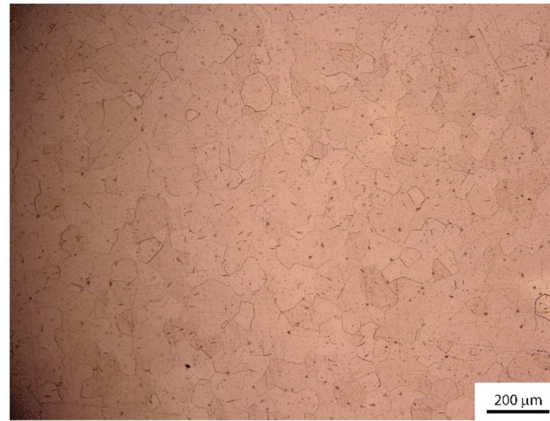


**Figure 2.** A schematic diagram of the laser system.

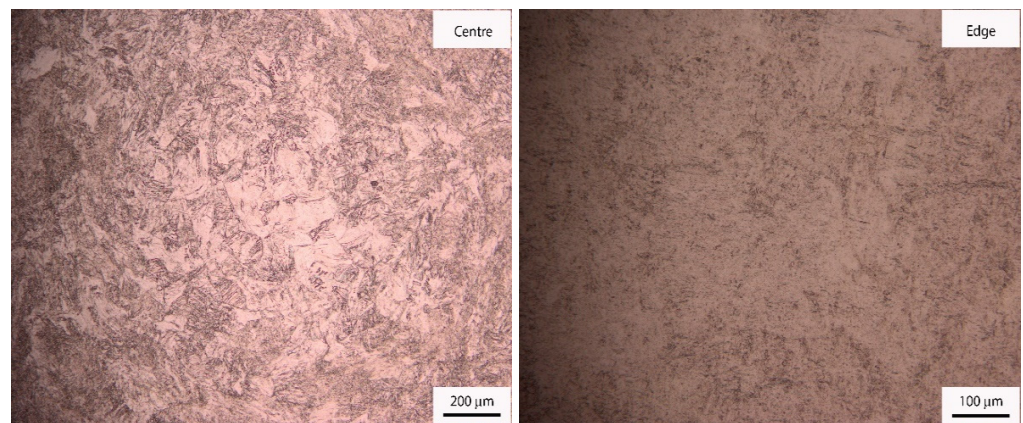
The surface morphologies of the various laser-treated samples were examined using an optical microscope (HRM-300, Huvitz, Gyeonggi-do, Korea). The hydrophilic/hydrophobic properties of the surface-modified samples were investigated by measuring the contact angles of droplets of de-ionized water with volumes of 1  $\mu\text{L}$ . In these experiments the contact angle and roughness were measured three times and the average value was used for comparison purposes. The roughness of the laser-modified samples was measured using an Alpha step profiler (D-300, KLA, Milpitas, CA, USA) with a scanning speed of 0.4 mm s<sup>-1</sup>, a scan line length of 5 mm and a load of 10 mg. The content of element C was measured using analysis with an Auger electron nanoscope (ULVAC-PHI, PHI 700, Kanagawa, Japan). The laser-treated surfaces were observed over a period from 1 to 27 days in order to fully evaluate the evolution of the surface hydrophilic or hydrophobic characteristics. The surface morphology of laser-modified samples was observed by a field-emission scanning electron microscope (SEM) with model JSM-7600F (JEOL Ltd., Tokyo, Japan). The microstructures of the Ti-6Al-4V alloy and the surface-modified specimens were examined by X-ray Diffractometer (XRD, Bruker D8 Advance, Karlsruhe, Germany). The 2 theta ranges are 20–80 deg and the step mode is 0.03 deg and 0.4 s per step. It should be noted that Cu-K $\alpha$  radiation ( $\lambda = 0.154$  nm) at 40 kV and 40 mA was used.

### 3. Results

Figure 3 shows the microstructures of CP-Ti samples in the as-annealed state and after HPT processing to 10 and 20 turns by OM and TEM observations. In Figure 3a, the as-annealed CP-Ti has a coarse grain structure, with an average grain size of  $\sim 65 \mu\text{m}$  and an initial hardness value of  $\sim 157 \text{ Hv}$ .



(a)



(b)

(c)

Figure 3. Cont.

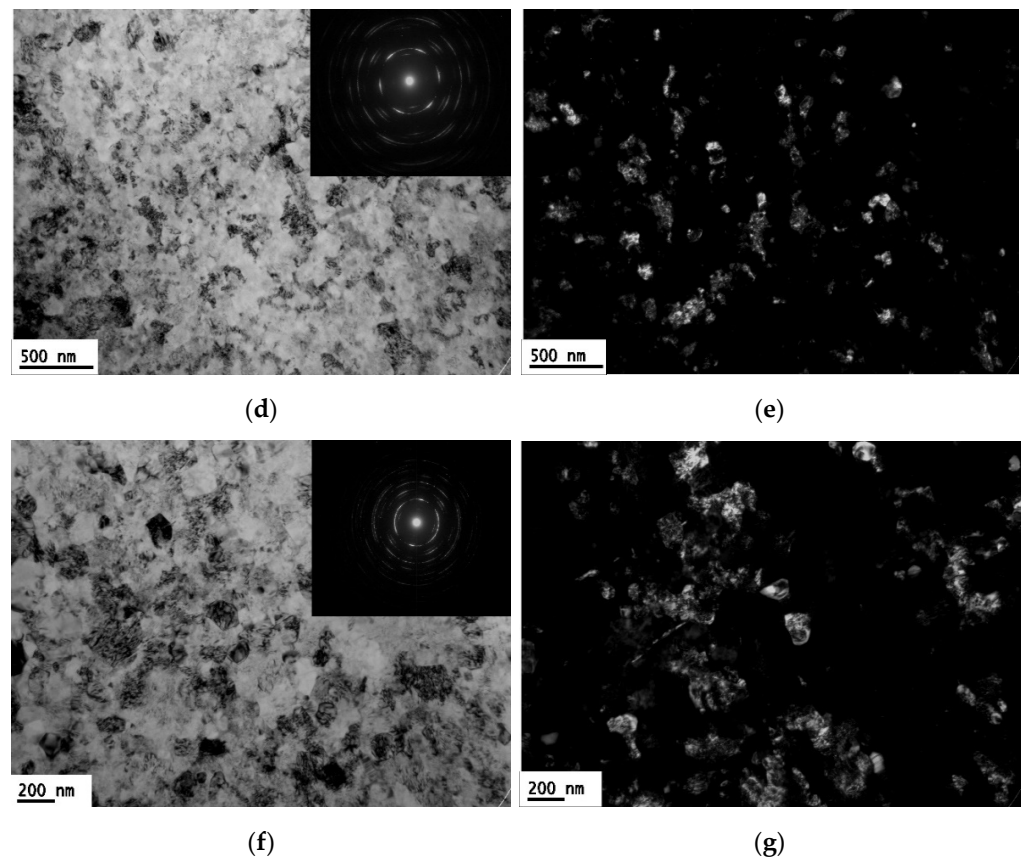


**Figure 3.** Microstructures of CP-Ti in (a) as-annealed state (OM image, magnification  $100\times$ ), and after HPT processing to (b) 1 turn in disc centre area (OM image, magnification  $100\times$ ), (c) 1 turn in disc edge area (OM image, magnification  $200\times$ ), (d,e) 10 turns  $\sim 4$  mm from disc edge area (TEM bright field and dark field images), (f,g) 20 turns  $\sim 4$  mm from disc edge area (TEM bright field and dark field images).

After HPT processing to 1 turn, as shown in Figure 3b,c, in the disc centre area, there remain some coarse grains but the torsional movement is visible because grains began to deform, which is different from the as-annealed CP-Ti sample in Figure 3a, whereas on the disc edge area it is more difficult to see grains under the optical microscope, even at higher magnification because of the heavy shear strain and subsequent grain refinement. The TEM microstructures of CP-Ti after 10 turns and 20 turns HPT processing are shown in Figure 3d–g, which include bright and dark field images. The SAD (selected area diffraction) patterns of 10 turns and 20 turns samples were inserted into the top-right corners in Figure 3d,f, respectively. As such, 10 and 20 turns HPT processing led to the formation of numerous high-angle grain boundaries and ultrafine grains, which are visible in the ring in the relevant SAD patterns. The shapes and sizes of the grains were found to be much easier to recognize in the corresponding dark field images, and from Figure 3e,g, it is clear that most of the ultrafine grains have equiaxed shapes. Further HPT processing, as shown in the TEM images in Figure 3d–g, demonstrate that significant grain refinement was achieved in CP-Ti, with a mean grain size of about  $70 \pm 18$  and  $60 \pm 12$  nm after 10 and 20 turns, respectively.

The initial microstructure of the Ti64 alloy after the two-step heat treatment is shown in Figure 4a,b, at two different magnifications, where lamellar ( $\alpha + \beta$ ) phases are present within the grains. The microstructure obtained by slow cooling from the  $\beta$  phase field contains individual  $\beta$  plates, separated by the remaining  $\beta$  matrix. In the low-magnification OM image in Figure 4a, there is a coarse grain structure with an average grain size of  $\sim 540 \mu\text{m}$ , whereas in the high-magnification OM image in Figure 4b, lamellar ( $\alpha + \beta$ )

phases are clearly visible with  $\alpha$  plates in a light colour and  $\beta$  plates in a dark colour, and the thicknesses of the coarse  $\alpha$  plates are in the range of  $\sim 2\text{--}6\ \mu\text{m}$ . Ti64 has an initial hardness value of  $\sim 309\ \text{Hv}$  for the heat-treated condition. After HPT processing to 1 turn, in the disc centre area, the coarse grains and lamellar structures within grains were deformed but they remain visible in Figure 4c, whereas in the disc edge area, most lamellar ( $\alpha + \beta$ ) phases were fragmented and only a small amount of lamellar ( $\alpha + \beta$ ) phases remained in sparse areas, but the grain structures are too small to be seen in the optical microscope in Figure 4d. After HPT processing for 10 turns, there was evidence for significant grain refinement, with a mean grain size of about  $50 \pm 10\ \text{nm}$  as shown in Figure 2e,f. The SAD pattern in Figure 4e became ring-like, thereby showing an evolution of grain structures into large numbers of high-angle boundaries.

For the CP-Ti and Ti64, a laser surface modification in an air atmosphere with a repetition rate of 25 kHz and a scanning speed of  $150\ \text{mm s}^{-1}$  was applied to the 20 turns HPT-processed samples (the N20 samples) and the heat-treated but unstrained samples (the N0 samples). The surface textures of laser-treated N0 and N20 samples of CP-Ti and Ti64 are displayed in Figure 5, from which valleys and hills can be observed on the sample surfaces. These are marks after the laser beam moves on the surface. Figure 6 shows the effect of different laser powers on the contact angle and surface roughness in both CP-Ti and Ti64. For the N0 samples, as shown in Figure 6a, the roughness of the Ti64 alloy was smaller than CP-Ti when the applied laser power was smaller than 2 W but the roughness of the Ti64 samples became larger than for CP-Ti when the laser power increased above  $\sim 3\ \text{W}$ . For the N20 samples, the roughness of Ti64 was significantly larger than for CP-Ti when the applied laser power was 5 W, as shown in Figure 6b. Figure 7 shows the observations of the surface morphology in the laser-treated zone of the laser-modified CP-Ti and Ti64 samples, with different holding times (1 day and 14 days), after applying a laser power of 5 W in an air atmosphere. Only 1 day after laser treatment, the surface morphology of Ti64 N20 samples showed more bumps than in CP-Ti N20 samples, as shown in Figure 7c,g, which confirms the larger roughness value of the Ti64 N20 sample than the CP-Ti N20 sample in Figure 6b. The roughness measurements in Figure 6a matched with the surface morphology observations in CP-Ti N0 and Ti64 N0 samples in Figure 7a,e as well, whereas, comparing Figure 6a,b, it is concluded that the roughness of the laser-treated N20 samples was rougher than for the N0 samples in Ti64 but there was no significant difference in the roughness values between the N20 and the N0 samples in CP-Ti. For the N20 samples, as shown in Figure 6b, the contact angles of Ti64 and CP-Ti were measured as  $\sim 11^\circ$  and  $\sim 17^\circ$ , respectively, when the applied laser power was 5 W. It is readily apparent that Ti64 is more hydrophilic than CP-Ti, for samples processed for 20 turns by HPT and, in addition, the N20 CP-Ti sample has both a lower roughness and a higher contact angle compared with the Ti64 alloy.

The SEM cross-section observations of laser-treated ultrafine-grained CP-Ti and Ti64 (HPT-processed N20 samples) are displayed in Figure 8. For the CP-Ti N20 sample, Figure 8a clearly shows the microstructure difference between the upper and bottom part of the cross section, where the upper part has a coarse-grained microstructure due to laser surface modification, whereas the bottom part is far from the surface and, therefore, the matrix ultrafine-grained microstructure remains. Measurements from Figure 8a demonstrate that microstructure coarsening occurred from the surface to about  $12\ \mu\text{m}$  in depth in the CP-Ti N20 sample. Similar microstructure coarsening phenomena were observed in the Ti64 N20 sample as well. The boundary between the coarse-grained and ultrafine-grained area is not very clear in Figure 8b, but it is still identifiable in the high-magnification image in Figure 8c. The microstructure coarsening due to laser modification on the Ti64 N20 sample occurred from the surface to a depth of about  $10\ \mu\text{m}$ .

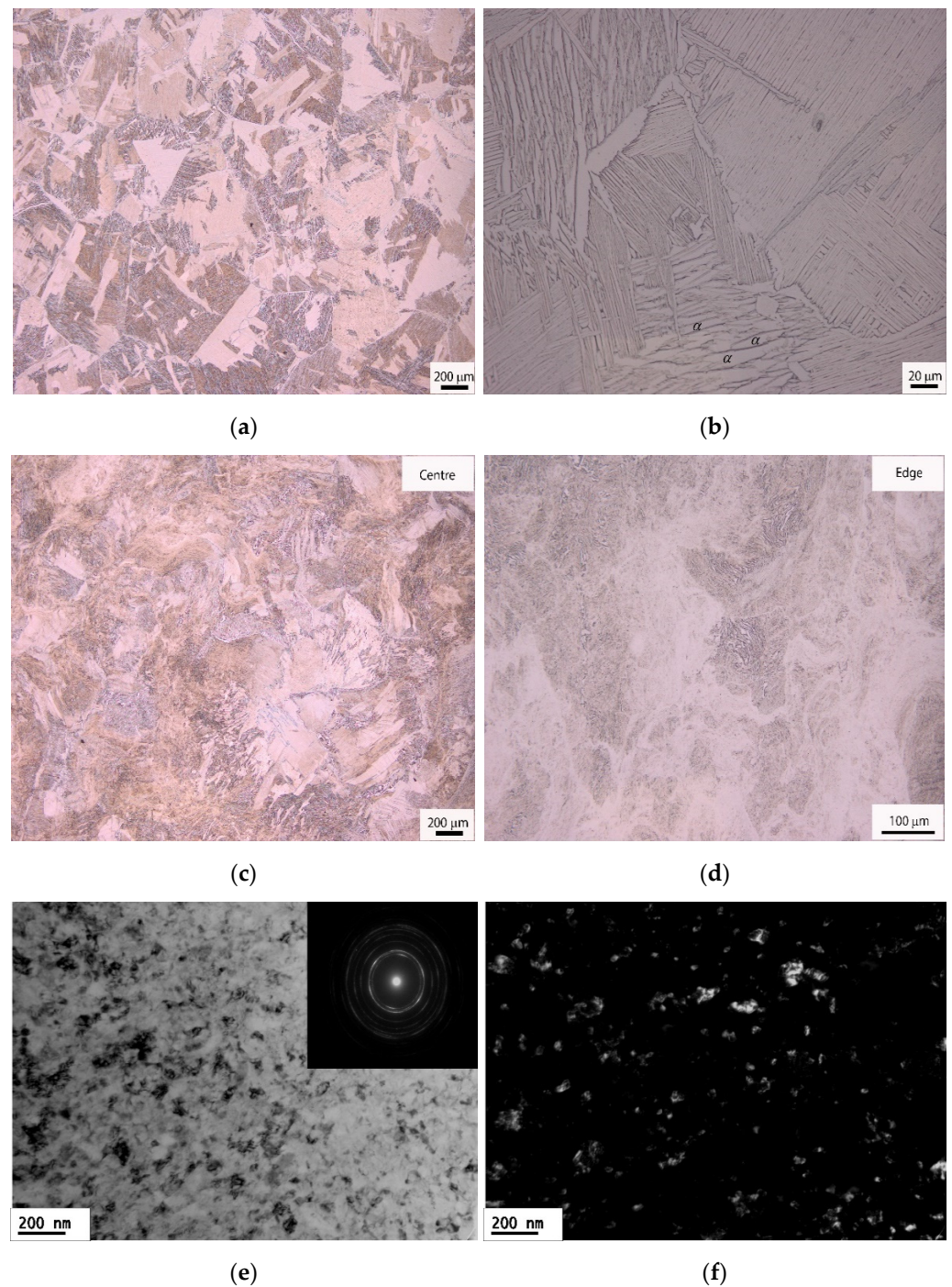


**Figure 4.** Microstructures of Ti64 in (a) as-heat-treated condition with low magnification (OM image, magnification 50×), (b) as-heat-treated condition with high magnification (OM image, magnification 500×) and after HPT processing (c) 1 turn in disc centre area (OM image, magnification 50×), (d) 1 turn in disc edge area (OM image, magnification 200×), (e,f) 10 turns at ~4 mm from disc edge area (TEM bright field and dark field image).



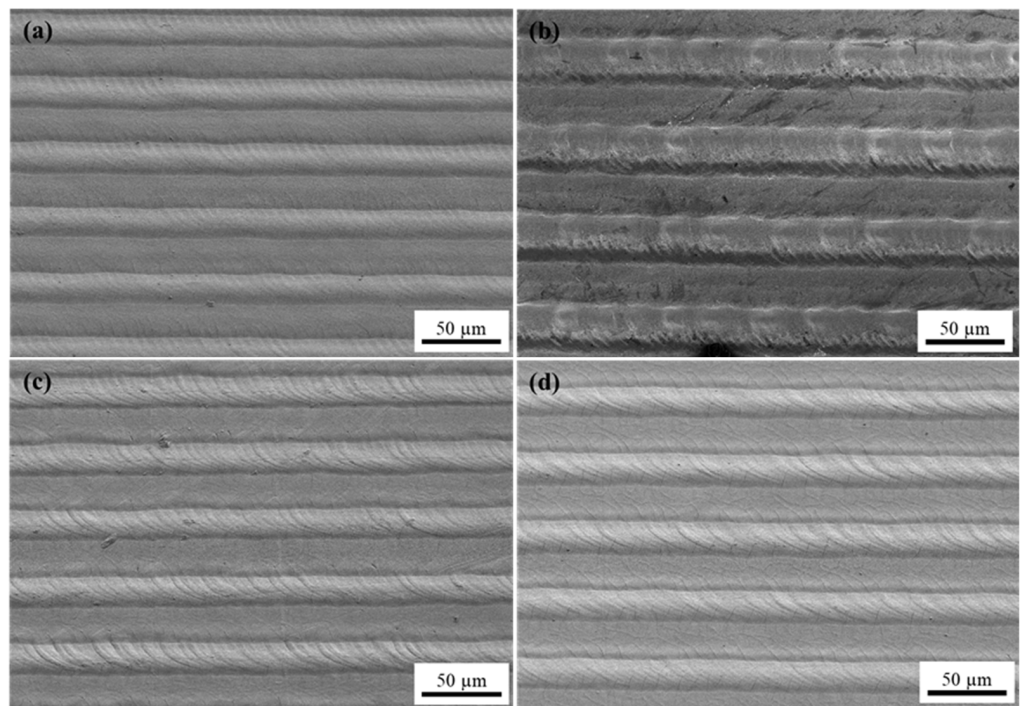


Figure 5. SEM images of the laser-textured surfaces in (a) CP-Ti N0, (b) CP-Ti N20, (c) Ti64 N0 and (d) Ti64 N20 samples.

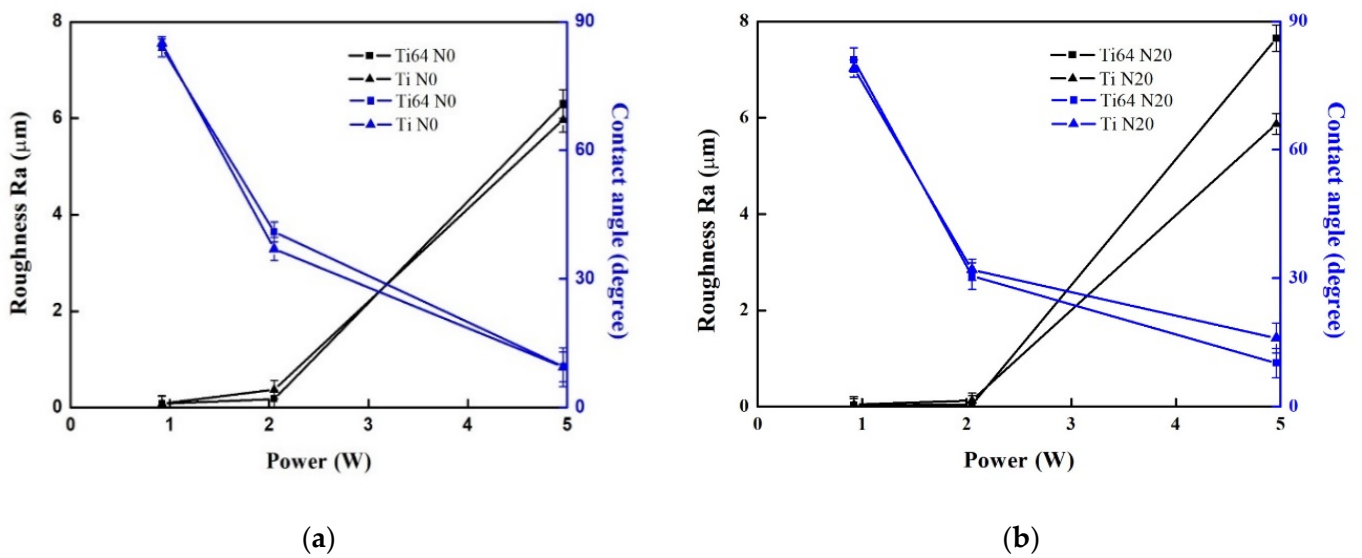
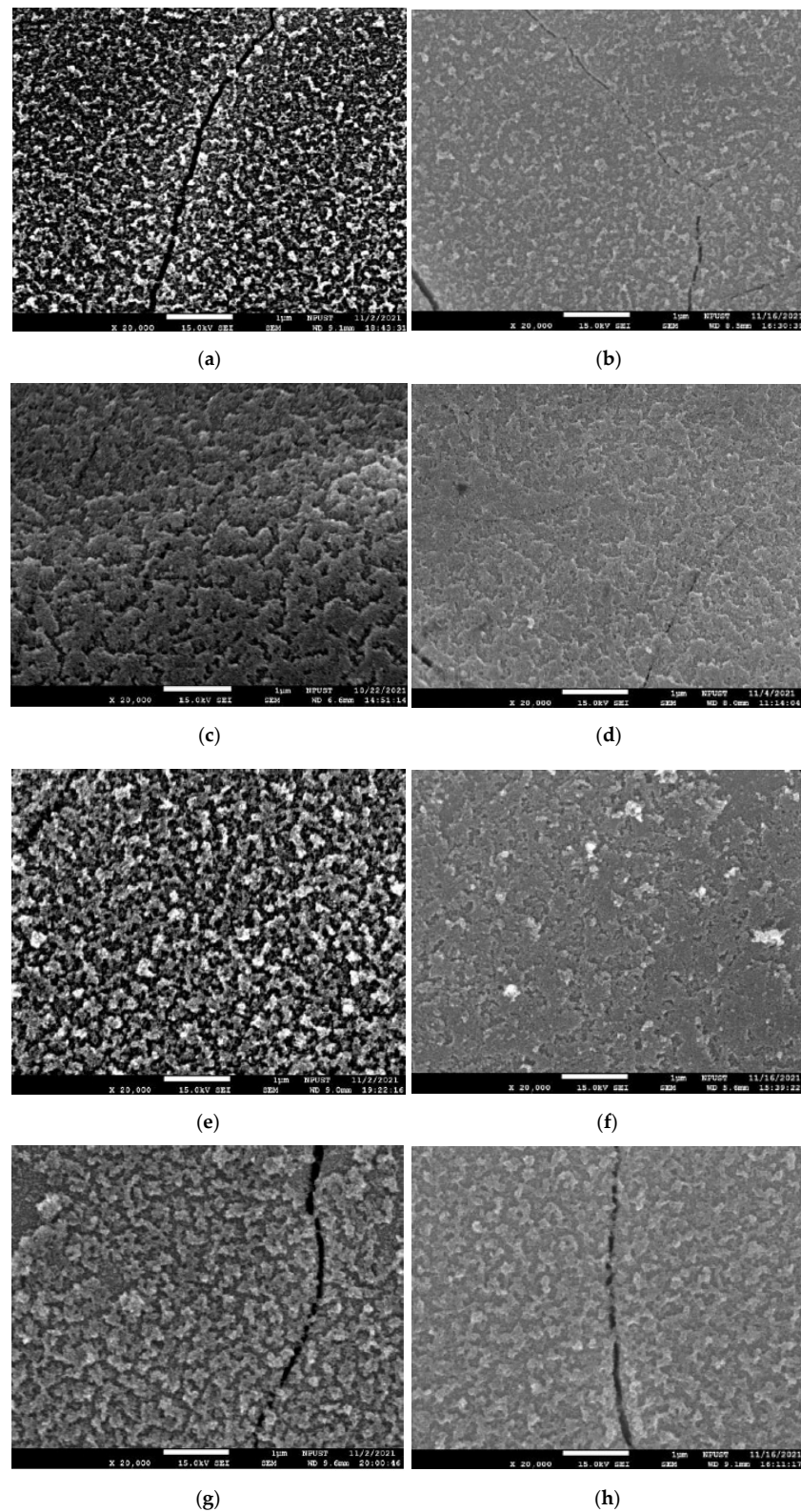
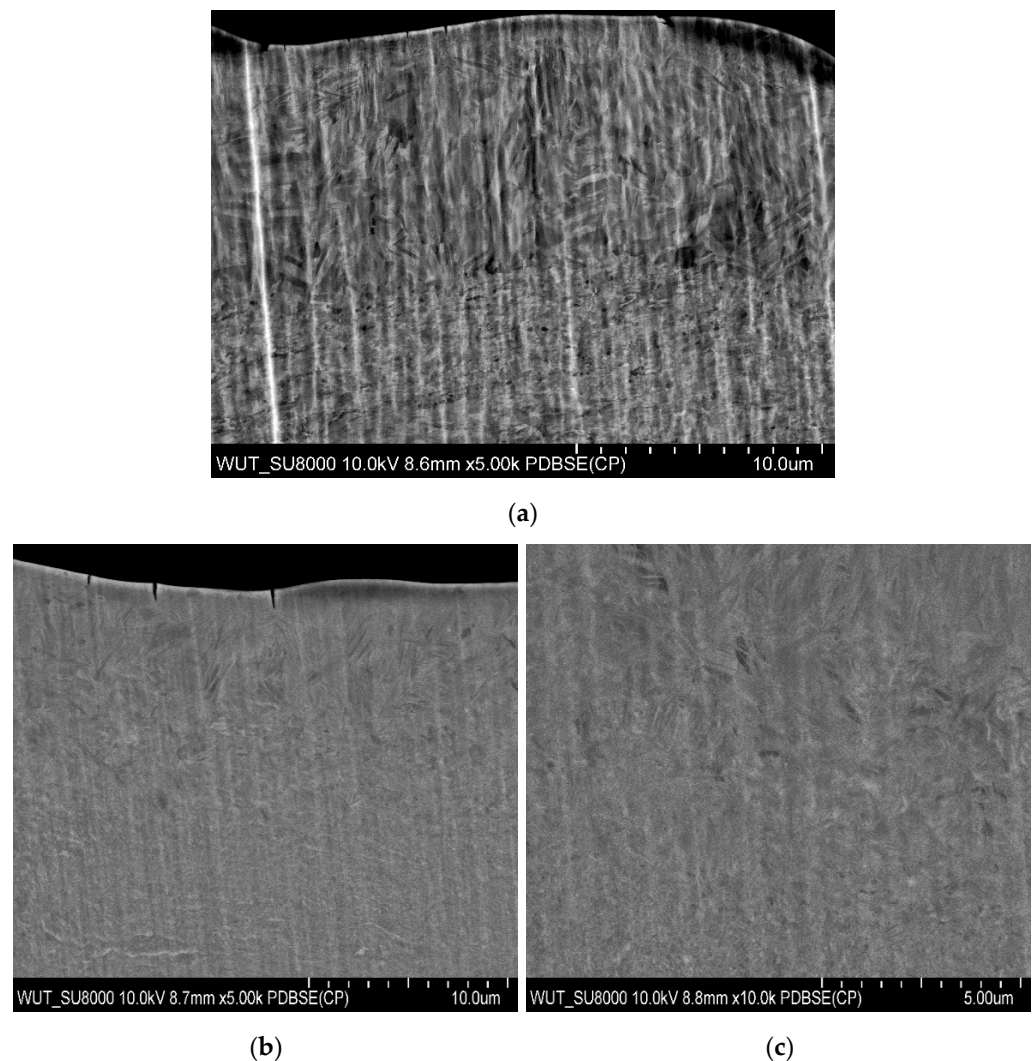


Figure 6. The roughness and contact angle of the CP-Ti and Ti64 samples for (a) N0 and (b) N20 after laser surface modification in an air atmosphere.



**Figure 7.** SEM images of the surface observations on laser-modified samples with different holding times (1 day and 14 days) after applying 5 W laser power in air atmosphere (a) CP-Ti N0 sample, 1 day, (b) CP-Ti N0 sample, 14 days, (c) CP-Ti N20 sample, 1 day, (d) CP-Ti N20 sample, 14 days, (e) Ti64 N0 sample, 1 day, (f) Ti64 N0 sample, 14 days (g) Ti64 N20 sample, 1 day, (h) Ti64 N20 sample, 14 days.



**Figure 8.** SEM cross-sectional images of laser-modified samples after 14 days for (a) CP-Ti N20 sample, (b) Ti64 N20 sample (low magnification) and (c) Ti64 N20 sample (high magnification).

The XRD patterns of the HPT-processed and surface-modified Ti64 specimens at a laser power of 5 W are shown in Figure 9. Before HPT processing, the  $\beta(110)$  peak could be detected in the heat-treated but unstrained N0 sample. After HPT processing for 20 turns, the microstructure of Ti64 had a  $\beta$  phase with detected peaks of  $(10-10)\beta$ ,  $(0002)\beta$ ,  $(10-11)\beta$  and  $(10-12)\beta$ , but no  $\beta(110)$  peak was detected. The laser-treated Ti64 N20 sample showed a similar X-ray pattern as that of the HPT-processed N20 sample, but no obvious  $\text{TiO}_2$  structures were detected. Considering the low laser power applied (5 W) in the current research, it is assumed that the  $\text{TiO}_2$  layer could be too thin for detection by X-ray.

N0 samples of CP-Ti and Ti64 were selected for laser treatment under different atmospheres of vacuum, air and oxygen, with a laser power of 5 W and a scanning speed of  $150 \text{ mm s}^{-1}$ , in order to evaluate the effect of laser treatment atmosphere on surface modifications. The relationship between the contact angle and the holding time (in days) is shown in Figure 10. It is apparent that the surface contact angle increases with an increase in the holding time and the contact angle of laser-treated samples in a vacuum shows that the samples are more hydrophobic than those laser-treated in the  $\text{O}_2$  atmosphere. The contact angles of CP-Ti and Ti64 laser treated in a vacuum were  $140^\circ$  and  $145^\circ$ , respectively, after 27 days. By contrast, the contact angles of CP-Ti and Ti64 in the  $\text{O}_2$  atmosphere after 27 days were only  $22^\circ$  and  $68^\circ$ , respectively. Figure 11 shows the contact angle images for CP-Ti with different atmospheres after 27 days holding time, where it is apparent that

laser-treated CP-Ti in an O<sub>2</sub> atmosphere has a smaller contact angle than when laser treated in vacuum and air atmospheres. It is necessary to mention that any given atmosphere (air, vacuum and O<sub>2</sub>) laser treatment and with an increase in the subsequent holding time can lead to a transformation from hydrophilic-to-hydrophobic properties.

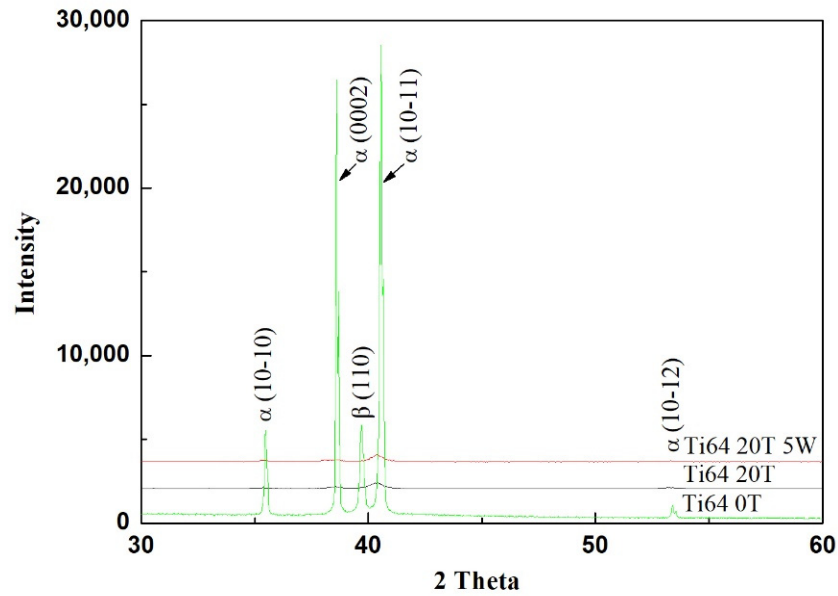


**Figure 9.** XRD spectra of the heat-treated but unstrained N0 sample, HPT-processed N20 sample and the surface-modified N20 sample of Ti64 at a laser power of 5 W.

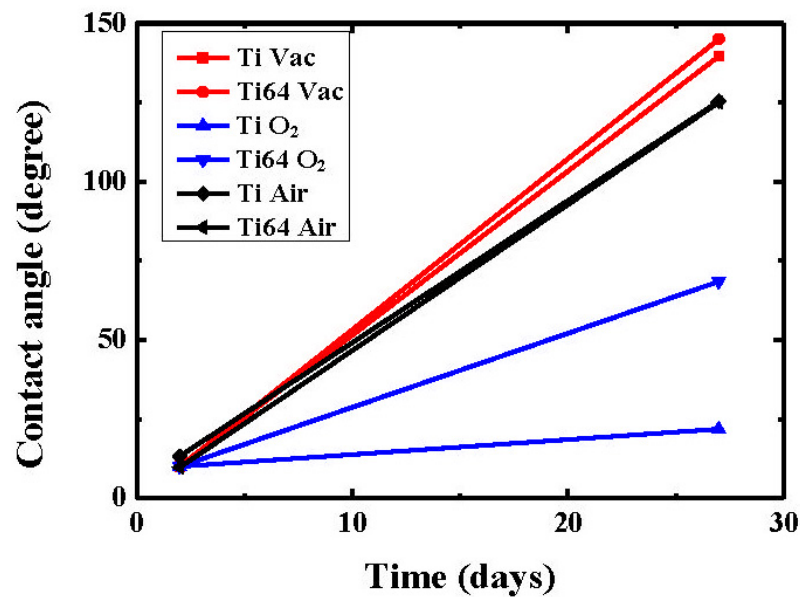


**Figure 10.** The contact angle versus the holding time (in days) for the N0 samples of CP-Ti and Ti64 measured separately in vacuum and oxygen atmospheres.

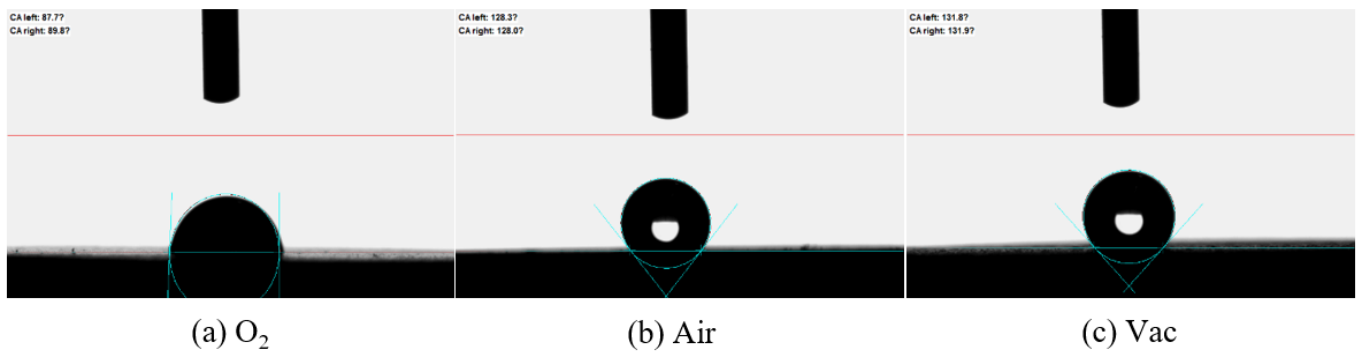


**Figure 11.** The contact angle images for CP-Ti with different atmospheres after 27 days holding time. (a) O<sub>2</sub>, (b) Air, (c) Vacuum.

According to the results in Figure 10, it is anticipated that the different atmospheres will produce different carbon and oxygen contents, as a study reported that different wettability was found to be a consequence of changes in surface chemistry [42]. Therefore, the various samples were examined using Auger electron nanoscope analysis. The relationship between the carbon and oxygen content and the holding time is shown for all samples in Figure 12. In Figure 12a, the variations in the carbon content with holding time is presented for the laser-treated CP-Ti and Ti64 in a vacuum and in an air atmosphere. Thus, when the surface carbon content of the CP-Ti sample is 47% after 27 holding days in Figure 12a, the contact angle reaches 140° (as shown in Figure 10) for laser treatment in the vacuum atmosphere. Comparing the carbon content in Figure 12a with the corresponding contact angles in Figure 10, the result demonstrates that the contact angle increases when the carbon content is higher. By contrast, laser treatment in the oxygen environment leads to a mass production of oxygen, as shown in Figure 12b, and then a reduction in the formation of carbon. In addition, the contact angle in the oxygen environment increases with increasing holding time at a lower rate than recorded in the vacuum or air atmospheres, as shown in Figure 10.

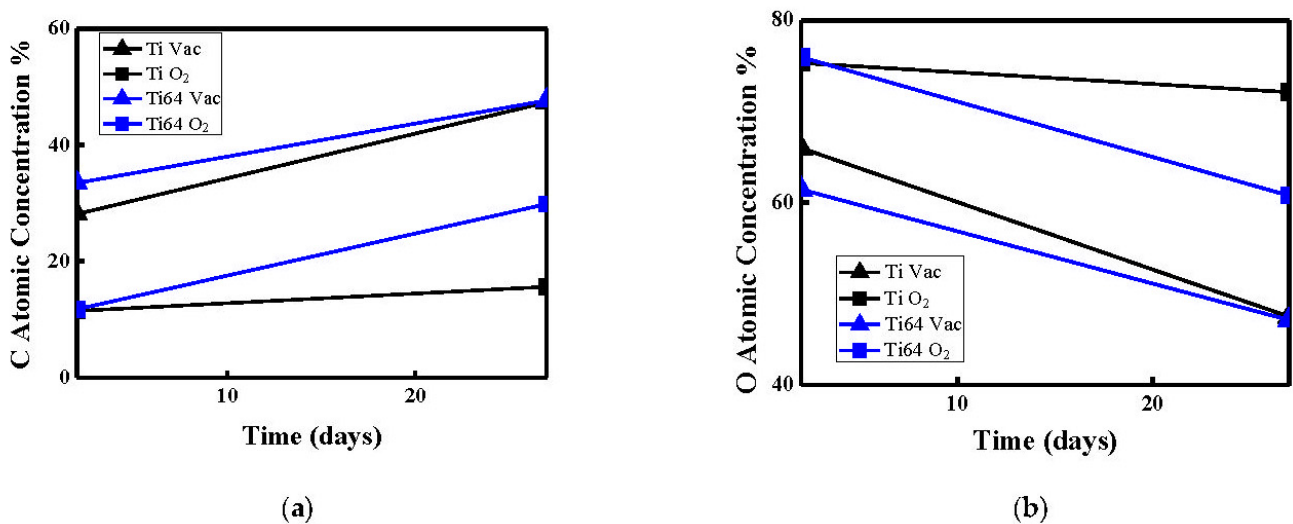


**Figure 12.** The variations in the concentration of chemical elements in the laser-modified surface with different holding times during different atmospheres in the N0 samples of CP-Ti and Ti64 for (a) the carbon content and (b) the oxygen content.

The N0 and N20 samples were treated in the air atmosphere with a laser power of 5 W and a scanning speed of 150 mm s<sup>-1</sup> in order to obtain different surface modifications. After the laser modification, the contact angles of the N0 and N20 CP-Ti samples were 13° and 10°, and for Ti64, the angles for the N0 and N20 samples were both equal to

10°. The relationships between the holding time and the measured contact angles for the CP-Ti and Ti64 samples placed in an air atmosphere are shown in Figure 13. It is readily apparent that, although there is some scatter in the individual datum points, the average contact angle of the N0 CP-Ti sample increased from 13° to 120° after 27 days and that of the N0 Ti64 sample increased from 10° to 117°. Obviously, laser treatment in air and subsequent holding for 27 days can lead the surface of treated samples to transform from hydrophilic to hydrophobic. Figure 7b,d,f,h shows the surface morphology after 14 days of laser treatment in the CP-Ti N0 sample, CP-Ti N20 sample, Ti64 N0 sample and Ti64 N20 sample. Comparing the surface morphology after 1 day of laser treatment with that after 14 days of laser treatment in Figure 7, it is found that the surface texture of each sample changed to less bumps and, therefore, contributed to high contact angles after 14 days. It is important to mention that the cracks in the surface morphology images shown in Figure 7 may be related to the laser power. There are several reports [50,51] that thermal input, shock waves and thermal accumulations would result in the form of cracking. In practice, these defects could be decreased by using femtosecond (short pulse width) or ultraviolet (short wavelength) lasers.

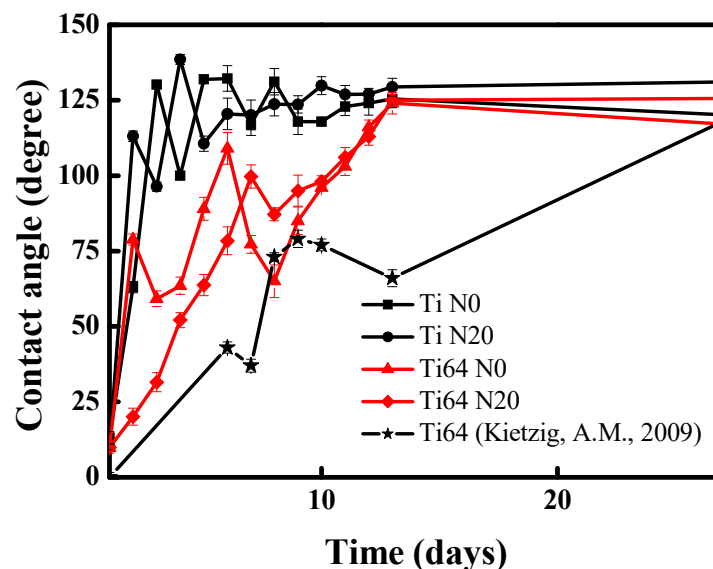


**Figure 13.** The relationship between the holding time and the measured values of the contact angles for CP-Ti and Ti64 samples treated in an air atmosphere with a laser power 5 W. ★ data in the figure is from [52].

#### 4. Discussion

The use of HPT processing was conducted in this research in order to produce an ultrafine-grained microstructure in CP-Ti and a Ti64 alloy. Lower numbers of HPT processing, for example, one turn of processing, led to a microstructure difference in the disc centre and edge area in both CP-Ti and Ti64, as shown in Figures 3b,c and 4c,d, which is consistent with a rigid body assumption that the strain imposed on the disc has a linear dependence on the distance from the disc centre and the strain is a maximum value at the outer edge of the disc [53]. It is seen that at the beginning of torsion, the accumulated plastic strain increases mostly at the edge of the sample, while it is nearly zero in the central portion of the sample. This region of zero strain shrinks gradually with the progress of straining. Strain gradient plasticity modelling of high-pressure torsion [54] confirms that five turns are sufficient to obtain a nearly uniform distribution of strain across the entire HPT sample. Therefore, as the HPT number of turns increase to 10 or 20 turns, samples should have more homogeneous microstructures along the disc diameter. The mean grain sizes of about  $70 \pm 18$  nm and  $\sim 60 \pm 12$  nm after 10 turns and 20 turns for the CP-Ti samples, as shown in Figure 3d–g, demonstrate that the nanostructured CP-Ti was produced through the heavy

shear deformation. There is a report that when the HPT number of turns is sufficiently high, it is possible to achieve a saturation in the ultrafine-grained microstructure [55]. Figure 4e–f shows that significant grain refinement occurred after 10 turns of the Ti64 sample, with a mean grain size of about  $50 \pm 10$  nm. However, the average hardness values after 10 and 20 turns for the Ti64 samples were measured as  $\sim 385$  Hv and  $\sim 390$  Hv, respectively, and this is consistent with the development of saturation in the microstructural conditions during HPT processing, so that it is reasonable to suggest the grain size in the 20 turns sample is similar to or even smaller than the grain size developed in the 10 turns sample.

It is obvious that, through HPT processing for 20 turns, nanogained structures were developed in both the CP-Ti and the Ti64 alloy, with both materials exhibiting significant grain refinements. Based on the analysis of the results in Figures 3 and 4, it is concluded that 20 turns of HPT processing will produce a mean grain size of about  $50 \pm 10$  nm or even smaller in Ti64, but in CP-Ti, the mean grain size is about  $60 \pm 12$  nm.

The surface of HPT-processed N20 samples (with nanogained microstructures) and heat-treated but unstrained N0 samples (with coarse-grained microstructures) was modified by the laser surface texturing in air to evaluate the influence of the laser processing parameters on the surface roughness and the hydrophilic/hydrophobic properties. After the laser surface texturing, the surface contact angle of all samples was hydrophilic, as shown in Figure 6. Comparing Figure 6a,b, there was no significant difference in the roughness values between the nanostructured N20 sample and the coarse-grained N0 sample of CP-Ti, but the nanostructured N20 sample showed a higher contact angle than the coarse-grained N0 sample. However, in Ti64, the roughness of the nanostructured N20 samples was rougher than for the coarse-grained N0 samples, but the nanostructured N20 sample showed a similar contact angle to the coarse-grained N0 sample. Obviously, nanostructured CP-Ti and Ti64 have slightly different responses to the laser treatment of corresponding coarse-grained materials. It is also apparent that the surface contact angle increases with an increase in the holding time for all samples treated in an air atmosphere, as displayed in Figure 13. Accordingly, it can be seen that when the surface roughness is increased in HPT-processed ultrafine-grained materials, so the surface contact angle changes from hydrophilic to super-hydrophilic. These phenomena are directly related to the traditional Wenzel model [33], in which the surface roughness directly affects the surface contact angle [56].

The coarse-grained CP-Ti and Ti64 (the N0 samples) were laser treated under different environments of vacuum, air and oxygen. Figure 10 shows that the contact angles of the samples laser treated in vacuum and air atmospheres are more hydrophobic than samples laser treated in an O<sub>2</sub> atmosphere. The rough surface geometry and the low-surface-energy chemical are widely known to be critical for achieving hydrophobicity, particularly on metal surfaces. In the O<sub>2</sub> atmosphere, the surface still absorbs organic compounds but the increasing rate of contact angle became slower than samples laser treated in vacuum and air atmospheres, with the result that the contact angles of CP-Ti and Ti64 are smaller than those of samples treated in vacuum and air atmospheres, as shown in Figure 10. Some early research reported that the change in hydrophobicity is not obvious in the atmosphere of O<sub>2</sub> [43–45] and this is similar to the current results in Figure 10 that laser-treated CP-Ti and Ti64 in an O<sub>2</sub> atmosphere have lower contact angles after 27 days holding. It can be concluded that the contact angles for both the CP-Ti and Ti64 samples increased with a change in the laser treatment atmosphere in the order of O<sub>2</sub>, air and vacuum. Several reports showed that a decomposition of carbon dioxide into carbon occurred during the pulsed laser treatment [52,57]. There is also a similar result showing that the surface with the highest carbon content has the highest contact angle [58]. Therefore, current research only focused on the analysis of oxygen and carbon content. The elemental analysis in Figure 12 shows that the oxygen content on the surface of the CP-Ti and Ti64 decreases and the carbon content increases with holding time. Accordingly, this corresponds to the contact angle increase with increasing holding time in the vacuum or air atmospheres in Figure 10. The laser processing showed a capability to tune the final

wetting behaviour by controlling the topography and modulating the chemical composition given by the processing environment [42]. Samples were oxidized after laser texturing and metal oxide shows hydrophilicity. The mechanism of wettability change was explained as a combined effect of micro-burr structure and surface chemistry [56]. It is obvious, therefore, that Ti is more easily combined with oxygen so that the carbon content on the surface decreases [59]. Therefore, laser modifications at different atmospheres produce different levels of contact angles and different rates of change for the transformations of the contact angles. This means that choosing the proper laser modification atmosphere will be a useful procedure in controlling both the contact angle transformation and the rate of occurrence of the transformation.

It is important to note that there exists a contact angle difference between laser-treated CP-Ti and Ti64 in the O<sub>2</sub> atmosphere after 27 days holding (Figure 10). In general, the higher the surface roughness, the larger the contact angle with increasing holding time. The roughness of the Ti64 N0 sample is higher than for the Ti N0 sample (shown in Figure 6) and, therefore, it is reasonable that the contact angle of the Ti64 N0 sample is larger than for Ti N0 in an O<sub>2</sub> atmosphere, as shown in Figure 10. In summary, the contact angles of CP-Ti and Ti64 are smaller than that of CP-Ti and Ti64 samples treated in vacuum and air atmospheres.

According to our previous result [23], the specimen was annealed at lower temperature (<500 °C) or lower laser power. No obvious structures were observed and the annealed thickness was thin. The XRD patterns of the annealed Ti-6Al-4V sample have a little TiO<sub>2</sub> structure. However, with an increase in the laser power, the titanium oxide layer grows more quickly, while the rutile phase becomes the main structure when the laser power is raised to 8.5 W. In this study, the laser power was 5 W and no obvious TiO<sub>2</sub> structures were observed. The annealed layer is thin so that the content of elemental C and O was measured using analysis with an Auger electron nanoscope.

It is apparent that the surface becomes rough via the laser surface modification and this produces a hydrophilic state. For the samples placed in the air atmosphere with different holding times, the surface gradually evolved from a hydrophilic to a hydrophobic state. It is important to note also that the oxygen content plays an important role in the wettability mechanism. Thus, in other studies on Ti-6Al-4V alloys, it was revealed that oxides formed over a period of days and this gave an increase in the Cassie-Baxter state contact angles due to multi-scale modifications [60]. In practice, the hydrophobic state occurs mainly through the formation of superimposed nanoscale and micrometre-sized corrugations and the carbon composition also increases with an increase in holding time. Thus, the hydrophobic surface is affected by the microtexture and chemical composition.

## 5. Summary and Conclusions

- (1) Samples of CP-Ti and Ti64 were successfully processed by up to 10 and 20 turns using high-pressure torsion in order to produce nanostructured microstructures. Mean grain sizes of about  $70 \pm 18$  and  $60 \pm 12$  nm were developed in CP-Ti after 10 and 20 turns, respectively. The Ti64 had a mean grain size of about  $50 \pm 10$  nm after HPT processing for 10 turns.
- (2) Laser surface modifications were applied on HPT-processed for 20 turns CP-Ti and Ti64 samples. With an applied laser power of 5 W, the measured contact angles of Ti64 and CP-Ti were  $\sim 11^\circ$  and  $\sim 17^\circ$ , respectively, so it is readily apparent that Ti64 is more hydrophilic than CP-Ti for samples processed for 20 turns by HPT. The laser-modified surface became hydrophilic, the contact angle increased with an increase in the holding time and the surface transformed gradually from a hydrophilic state to a hydrophobic state.
- (3) Laser surface modifications were applied in three different atmospheres of vacuum, air and oxygen on coarse-grained CP-Ti and Ti64 samples. The contact angles increased with the carbon content concentrations in both CP-Ti and Ti64 due to the change in the laser treatment atmospheres. The slow formation of carbon produced a rapid increase



in contact angle in a vacuum environment. The rate of increase in the contact angle in the oxygen environment was also greatly reduced. The maximum contact angle could reach 140° in a vacuum atmosphere. This study describes a simple method that can be employed to fabricate a hydrophobic surface for use in medical devices.

**Author Contributions:** Conceptualization, H.-K.L., Y.H. and T.G.L.; methodology and HPT processing, J.M. and Y.H.; microstructure investigation, P.B. and J.M.; laser treatment and surface observation, H.-K.L., Y.-H.C., G.-Y.L. and Y.-C.C.; writing and editing, H.-K.L., Y.H. and T.G.L. All authors have read and agreed to the published version of the manuscript.

**Funding:** This research was funded by the Ministry of Science and Technology of Taiwan under Grant No. MOST 109-2927-I-020-501 and by the Royal Society in the UK under Grant No. IEC\R3\193025.

**Data Availability Statement:** The data sets used or analyzed in the current study are available from the corresponding author upon reasonable request.

**Conflicts of Interest:** The authors declare no conflict of interest.

## References

1. Balazic, M.; Kopac, J.; Jackson, M.J.; Ahmed, W. Review: Titanium and titanium alloy applications in medicine. *Int. J. Nano Biomater.* **2008**, *1*, 3–34. [[CrossRef](#)]
2. Li, Y.; Yang, C.; Zhao, H.; Qu, S.; Li, X.; Li, Y. New developments of Ti-based alloys for biomedical applications. *Materials* **2014**, *7*, 1709–1800. [[CrossRef](#)] [[PubMed](#)]
3. Figueiredo, R.B.; de C. Barbosa, E.R.; Zhao, X.; Yang, X.; Liu, X.; Cetlin, P.R.; Langdon, T.G. Improving the fatigue behavior of dental implants through processing commercial purity titanium by equal-channel angular pressing. *Mater. Sci. Eng.* **2014**, *A619*, 312–318. [[CrossRef](#)]
4. Sergueeva, A.V.; Stolyarov, V.V.; Valiev, R.Z.; Mukherjee, A.K. Advanced mechanical properties of pure titanium with ultrafine grained structure. *Scr. Mater.* **2001**, *45*, 747–752. [[CrossRef](#)]
5. Saito, Y.; Utsunomiya, H.; Tsuji, N.; Sakai, T. Novel ultra-high straining process for bulk materials—Development of the accumulative roll-bonding (ARB) process. *Acta Mater.* **1999**, *47*, 579–583. [[CrossRef](#)]
6. Valiev, R.Z.; Langdon, T.G. Principles of equal-channel angular pressing as a processing tool for grain refinement. *Prog. Mater. Sci.* **2006**, *51*, 881–981. [[CrossRef](#)]
7. Zhilyaev, A.P.; Langdon, T.G. Using high-pressure torsion for metal processing: Fundamentals and applications. *Prog. Mater. Sci.* **2008**, *53*, 893–979. [[CrossRef](#)]
8. Stolyarov, V.V.; Zhu, Y.T.; Alexandrov, I.V.; Lowe, T.C.; Valiev, R.Z. Influence of ECAP routes on the microstructure and properties of pure Ti. *Mater. Sci. Eng. A* **2001**, *299*, 59–67. [[CrossRef](#)]
9. Stolyarov, V.V.; Zhu, Y.T.; Lowe, T.C.; Valiev, R.Z. Microstructures and properties of ultrafine-grained pure titanium processed by equal-channel angular pressing and cold deformation. *J. Nanosci. Nanotechnol.* **2001**, *1*, 237–242. [[CrossRef](#)]
10. Wings-Ngam, J.; Kawasaki, M.; Langdon, T.G. A comparison of microstructures and mechanical properties in a Cu-Zr alloy processed using different SPD techniques. *J. Mater. Sci.* **2013**, *48*, 4653–4660. [[CrossRef](#)]
11. Sabbaghianrad, S.; Langdon, T.G. Developing superplasticity in an aluminum matrix composite processed by high-pressure torsion. *Mater. Sci. Eng. A* **2016**, *655*, 36–43. [[CrossRef](#)]
12. Shahmir, H.; He, J.; Lu, Z.; Kawasaki, M.; Langdon, T.G. Effect of annealing on mechanical properties of a nanocrystalline CoCrFeNiMn high-entropy alloy processed by high-pressure torsion. *Mater. Sci. Eng. A* **2016**, *676*, 294–303. [[CrossRef](#)]
13. Silva, C.L.P.; Soares, R.B.; Pereira, P.H.R.; Figueiredo, R.B.; Lins, V.F.C.; Langdon, T.G. The effect of high-pressure torsion on microstructure, hardness and corrosion behavior for pure magnesium and different magnesium alloys. *Adv. Eng. Mater.* **2019**, *21*, 1801081. [[CrossRef](#)]
14. Lin, H.; Huang, J.; Langdon, T.G. Relationship between texture and low temperature superplasticity in an extruded AZ31 Mg alloy processed by ECAP. *Mater. Sci. Eng. A* **2005**, *402*, 250–257. [[CrossRef](#)]
15. Huang, Y.; Figueiredo, R.B.; Baudin, T.; Brisset, F.; Langdon, T.G. Evolution of strength and homogeneity in a magnesium AZ31 alloy processed by high-pressure torsion at different temperatures. *Adv. Eng. Mater.* **2012**, *14*, 1018–1026. [[CrossRef](#)]
16. Niekil, F.; Schweizer, P.; Kraschewski, S.M.; Butz, B.; Spiecker, E. The process of solid-state dewetting of Au thin films studied by in situ scanning transmission electron microscopy. *Acta Mater.* **2015**, *90*, 118–132. [[CrossRef](#)]
17. Wang, M.; Yang, Z.; Yang, C.; Zhang, D.; Tian, Y.; Liu, X. The investigation of mechanical and thermal properties of superhydrophobic nitinol surfaces fabricated by hybrid methods of laser irradiation and carbon ion implantation. *Appl. Surf. Sci.* **2020**, *527*, 146889. [[CrossRef](#)]
18. Dongre, G.; Rajurkar, A.; Raut, R.; Jangam, S. Preparation of super-hydrophobic textures by using nanosecond pulsed laser. *Mater. Today Proc.* **2021**, *42*, 1145–1151. [[CrossRef](#)]
19. Luo, B.; Shum, P.W.; Zhou, Z.; Li, K. Preparation of hydrophobic surface on steel by patterning using laser ablation process. *Surf. Coat. Technol.* **2010**, *204*, 1180–1185. [[CrossRef](#)]

20. Kwon, M.H.; Shin, H.S.; Chu, C.N. Fabrication of a super-hydrophobic surface on metal using laser ablation and electrodeposition. *Appl. Surf. Sci.* **2014**, *288*, 222–228. [[CrossRef](#)]
21. Oh, Y.; Lee, M. Single-pulse transformation of Ag thin film into nanoparticles via laser-induced dewetting. *Appl. Surf. Sci.* **2017**, *399*, 555–564. [[CrossRef](#)]
22. Raimbault, O.; Benayoun, S.; Anselme, K.; Mauclair, C.; Bourgade, T.; Kietzig, A.-M.; Girard-Lauriault, P.-L.; Valette, S.; Donnet, C. The effects of femtosecond laser-textured Ti-6Al-4V on wettability and cell response. *Mater. Sci. Eng. C* **2016**, *69*, 311–320. [[CrossRef](#)] [[PubMed](#)]
23. Hong, T.F.; Chi, K.P.; Lin, H.K.; Wu, Y.D. Laser surface modification for rapid oxide layer formation on Ti-6Al-4V. *J. Laser Micro Nanoeng.* **2014**, *9*, 64–67. [[CrossRef](#)]
24. Moritz, N.; Areva, S.; Wolke, J.; Peltola, T. TF-XRD examination of surface-reactive TiO<sub>2</sub> coatings produced by heat treatment and CO<sub>2</sub> laser treatment. *Biomaterials* **2005**, *26*, 4460–4467. [[CrossRef](#)] [[PubMed](#)]
25. Elias, C.N.; Oshida, Y.; Lima, J.H.; Muller, C.A. Relationship between surface properties (roughness, wettability and morphology) of titanium and dental implant removal torque. *J. Mech. Behav. Biomed. Mater.* **2008**, *1*, 234–242. [[CrossRef](#)]
26. Ponsoy, L.; Reybier, K.; Jaffrezic, N.; Comte, V.; Lagneau, C.; Lissac, M.; Martelet, C. Relationship between surface properties (roughness, wettability) of titanium and titanium alloys and cell behaviour. *Mater. Sci. Eng. C* **2003**, *23*, 551–560. [[CrossRef](#)]
27. Apreutesei, M.; Billard, A.; Steyer, P. Crystallization and hardening of Zr-40 at.% Cu thin film metallic glass: Effects of isothermal annealing. *Mater. Des.* **2015**, *86*, 555–563. [[CrossRef](#)]
28. Liu, X.; Chu, P.K.; Ding, C. Surface modification of titanium, titanium alloys, and related materials for biomedical applications. *Mater. Sci. Eng. R Rep.* **2004**, *47*, 49–121. [[CrossRef](#)]
29. Zulfiqar, U.; Hussain, S.Z.; Awais, M.; Khan, M.M.J.; Hussain, I.; Husain, S.W.; Subhani, T. In-situ synthesis of bi-modal hydrophobic silica nanoparticles for oil-water separation. *Colloids Surf. A Physicochem. Eng. Asp.* **2016**, *508*, 301–308. [[CrossRef](#)]
30. Fu, J.; Zhu, Y.; Zheng, C.; Liu, R.; Ji, Z. Evaluate the effect of laser shock peening on plasticity of Zr-based bulk metallic glass. *Opt. Laser Technol.* **2015**, *73*, 94–100. [[CrossRef](#)]
31. Yilbas, B.S.; Ali, H. Laser texturing of Hastelloy C276 alloy surface for improved hydrophobicity and friction coefficient. *Opt. Lasers Eng.* **2016**, *78*, 140–147. [[CrossRef](#)]
32. Lin, H.K.; Li, G.Y.; Mortier, S.; Bazarnik, P.; Huang, Y.; Lewandowska, M.; Langdon, T.G. Processing of CP-Ti by high-pressure torsion and the effect of surface modification using a post-HPT laser treatment. *J. Alloy. Compd.* **2019**, *784*, 653–659. [[CrossRef](#)]
33. Wenzel, R.N. Resistance of solid surfaces to wetting by water. *Ind. Eng. Chem.* **1936**, *28*, 988–994. [[CrossRef](#)]
34. Cassie, A.; Baxter, S. Wettability of porous surfaces. *Trans. Faraday Soc.* **1944**, *40*, 546–551. [[CrossRef](#)]
35. David, R.; Neumann, A.W. Energy barriers between the Cassie and Wenzel states on random, superhydrophobic surfaces. *Colloids Surf. A Physicochem. Eng. Asp.* **2013**, *425*, 51–58. [[CrossRef](#)]
36. Takeda, S.; Fukawa, M.; Hayashi, Y.; Matsumoto, K. Surface OH group governing adsorption properties of metal oxide films. *Thin Solid Film.* **1999**, *339*, 220–224. [[CrossRef](#)]
37. Yang, C.J.; Mei, X.S.; Tian, Y.I.; Zhang, D.W.; Li, Y.; Liu, X.P. Modification of wettability property of titanium by laser texturing. *Int. J. Adv. Manuf. Technol.* **2016**, *87*, 1663–1670. [[CrossRef](#)]
38. Vidhya, Y.E.B.; Pattamatta, A.; Manivannan, A.; Vasa, N.J. Influence of fluence, beam overlap and aging on the wettability of pulsed Nd<sup>3+</sup>: YAG nanosecond laser-textured Cu and Al sheets. *Appl. Surf. Sci.* **2021**, *548*, 149259. [[CrossRef](#)]
39. Ta, D.V.; Dunn, A.; Wasley, T.J.; Kay, R.W.; Stringer, J.; Smith, P.J.; Connaughton, C.; Shephard, J.D. Nanosecond laser textured superhydrophobic metallic surfaces and their chemical sensing applications. *Appl. Surf. Sci.* **2015**, *357*, 248–254. [[CrossRef](#)]
40. Ta, V.D.; Dunn, A.; Wasley, T.J.; Li, J.; Kay, R.W.; Stringer, J.; Smith, P.J.; Esenturk, E.; Connaughton, C.; Shephard, J.D. Laser textured superhydrophobic surfaces and their applications for homogeneous spot deposition. *Appl. Surf. Sci.* **2016**, *365*, 153–159. [[CrossRef](#)]
41. Guan, Y.C.; Luo, F.F.; Lim, G.C.; Hong, M.H.; Zheng, H.Y.; Qi, B. Fabrication of metallic surfaces with long-term superhydrophilic property using one-stop laser method. *Mater. Des.* **2015**, *78*, 19–24. [[CrossRef](#)]
42. Pou, P.; del Val, J.; Riveiro, A.; Comesaña, R.; Arias-González, F.; Lusquiños, F.; Bountinguiza, M.; Quintero, F.; Pou, J. Laser texturing of stainless steel under different processing atmospheres: From superhydrophilic to superhydrophobic surfaces. *Appl. Surf. Sci.* **2019**, *475*, 896–905. [[CrossRef](#)]
43. Samanta, A.; Wang, Q.; Shaw, S.K.; Ding, H. Roles of chemistry modification for laser textured metal alloys to achieve extreme surface wetting behaviors. *Mater. Des.* **2020**, *192*, 108744. [[CrossRef](#)]
44. Liu, M.; Yang, Z.; Dong, L.; Wang, Z.; Wang, S.; Wang, L.; Xie, Y.; Zhang, Q.; Weng, Z.; Tian, T. Vacuum conditions for tunable wettability transition on laser ablated Ti-6Al-4V alloy surfaces. *Colloids Surf. A Physicochem. Eng. Asp.* **2022**, *647*, 129023. [[CrossRef](#)]
45. Shi, Y.; Jiang, Z.; Cao, J.; Ehmann, K.F. Texturing of metallic surfaces for superhydrophobicity by water jet guided laser micro-machining. *Appl. Surf. Sci.* **2020**, *500*, 144286. [[CrossRef](#)]
46. Huang, Y.; Mortier, S.; Pereira, P.H.R.; Bazarnik, P.; Lewandowska, M.; Langdon, T.G. Thermal stability and mechanical properties of HPT-processed CP-Ti. *IOP Conf. Ser. Mater. Sci. Eng.* **2017**, *194*, 012012. [[CrossRef](#)]
47. Xu, C.; Horita, Z.; Langdon, T.G. The evolution of homogeneity in an aluminum alloy processed using high-pressure torsion. *Acta Mater.* **2008**, *56*, 5168–5176. [[CrossRef](#)]

48. Figueiredo, R.B.; Cetlin, P.R.; Langdon, T.G. Using finite element modeling to examine the flow processes in quasi-constrained high-pressure torsion. *Mater. Sci. Eng. A* **2011**, *528*, 8198–8204. [[CrossRef](#)]
49. Figueiredo, R.B.; Pereira, P.H.R.; Aguilar, M.T.P.; Cetlin, P.R.; Langdon, T.G. Using finite element modeling to examine the temperature distribution in quasi-constrained high-pressure torsion. *Acta Mater.* **2012**, *60*, 3190–3198. [[CrossRef](#)]
50. Eberle, G.; Schmidt, M.; Pude, F.; Wegener, K. Laser surface and subsurface modification of sapphire using femtosecond pulse. *Appl. Surf. Sci.* **2016**, *378*, 504–512. [[CrossRef](#)]
51. Fu, J.; Zhu, Y.; Zheng, C.; Liu, R.; Ji, R. Effect of laser shock peening on mechanical properties of Zr-based bulk metallic glass. *Appl. Surf. Sci.* **2014**, *313*, 692–697. [[CrossRef](#)]
52. Kietzig, A.-M.; Hatzikriakos, S.G.; Englezos, P. Patterned superhydrophobic metallic surfaces. *Langmuir* **2009**, *25*, 4821–4827. [[CrossRef](#)]
53. Valiev, R.Z.; Ivanisenko, Y.V.; Rauch, E.F.; Baudalet, B. Structure and deformation behaviour of Armco iron subjected to severe plastic deformation. *Acta Mater.* **1996**, *44*, 4705–4712. [[CrossRef](#)]
54. Estrin, Y.; Molotnikov, A.; Davies, C.H.J.; Lapovok, R. Strain gradient plasticity modelling of high-pressure torsion. *J. Mech. Phys. Solids* **2008**, *56*, 1186–1202. [[CrossRef](#)]
55. Sabbaghianrad, S.; Langdon, T.G. An evaluation of the saturation hardness in an ultrafine-grained aluminum 7075 alloy processed using different techniques. *J. Mater. Sci.* **2015**, *50*, 4357–4365. [[CrossRef](#)]
56. Yeh, K.Y.; Chen, L.J.; Chang, J.Y. Contact angle hysteresis on regular pillar-like hydrophobic surfaces. *Langmuir* **2008**, *24*, 245–251. [[CrossRef](#)] [[PubMed](#)]
57. Ngo, C.-V.; Chun, D.-M. Fast wettability transition from hydrophilic to superhydrophobic laser-textured stainless steel surfaces under low-temperature annealing. *Appl. Surf. Sci.* **2017**, *409*, 232–240. [[CrossRef](#)]
58. Huerta-Murillo, D.; García-Girón, A.; Romano, J.M.; Cardoso, J.T.; Cordovilla, F.; Walker, M.; Dimov, S.S.; Ocaña, J.L. Wettability modification of laser-fabricated hierarchical surface structures in Ti-6Al-4V titanium alloy. *Appl. Surf. Sci.* **2019**, *463*, 838–846. [[CrossRef](#)]
59. Liu, Z.; Welsch, G. Literature survey on diffusivities of oxygen, aluminum, and vanadium in alpha titanium, beta titanium, and in rutile. *Metall. Trans. A* **1988**, *19A*, 1121–1125. [[CrossRef](#)]
60. Zeng, Q. Size matching effect on Wenzel wetting on fractal surfaces. *Results Phys.* **2018**, *10*, 588–593. [[CrossRef](#)]